Applied Physics Letters, Vol. 111, Issue 25, 2017, Article number 253103
DOI:10.1063/1.4997774

Chemical vapour deposition of freestanding sub-60 nm graphene gyroids

Tomasz Cebo,[†] Adrianus I. Aria,[†§] James A. Dolan[†‡≡], Robert S. Weatherup,[†] Kenichi Nakanishi,[†] Piran R. Kidambi, [Δ] Giorgio Divitini, [ϟ] Caterina Ducati, [ϟ] Ullrich Steiner[≡] and Stephan Hofmann[†*]

[†] Department of Engineering, University of Cambridge, United Kingdom CB3 0FA

[‡] Department of Physics, University of Cambridge, United Kingdom CB3 0HE

[§] Surface Engineering and Nanotechnology Institute, Cranfield University, United Kingdom MK43 0AL

[Δ] Department of Chemical and Biomolecular Engineering, Vanderbilt University School of Engineering, 2301 Vanderbilt Place PMB 351826. Nashville, TN 37235-1826, USA.

[ϟ] Department of Materials Science and Metallurgy, University of Cambridge, United Kingdom CB3 0FS

[≡] Adolphe Merkle Institute, University of Fribourg, Switzerland, CH-1700

Abstract

Gyroidal graphene nanostructures allow the engineering of unique physical properties and are of interest to applications ranging from energy storage and catalysis to filtration, thermal management and sensing. However, despite recent advances, the synthesis of a free-standing graphene assembly with a non-stochastic, sub-micron unit cell has proven challenging due to the difficulties in template manufacture and structural stability throughout a high-temperature chemical vapour deposition (CVD) process. Here we demonstrate the direct CVD synthesis of freestanding graphene gyroids with controlled sub-60nm unit cell sizes. We fabricate three-dimensional (3D) nickel templates through electrodeposition into a selectively voided triblock terpolymer and effectively address the high temperature instabilities of such sub-micron unit cell structures via the early introduction of carbon precursor, which stabilizes the metallized gyroidal templates. The as-grown graphene gyroids are self-supporting and can be transferred onto a variety of substrates. Furthermore they represent the smallest free standing graphene 3D structures yet produced with a pore size of tens of nm. We analyse their structure by electron microscopy and optical spectroscopy. We discuss the generality of our methodology for the synthesis of other types of nanoscale, 3D graphene assemblies and the transferability of this approach to other 2D materials.

Keywords: gyroid, graphene foam, free-standing graphene, graphene nanostructure, CVD, template stability, precursor predosing, block copolymer self-assembly

[*] Corresponding author: sh315@cam.ac.uk

Introduction

2D materials not only offer unique functionality as planar atomically thin layers but can also be engineered into complex 3D structures, allowing the design of a new class of materials with tailored mechanical, thermal, electrical and optical properties, ultra-low density and high surface area. Recent literature highlights the promise of such new porous, foam-like materials, in particular those derived from graphene, in applications ranging from (opto)electronics,[1,2] artificial skin,[3] electrochemistry,[4–6] and catalysis[7] to thermal management,[8] self-cleaning,[9] sorption and filtration,[10] sensors,[11] bio-medical[12] and mechanical metamaterials.[13,14] Among the various synthetic strategies and 3D assembly approaches,[15] chemical vapour deposition (CVD) has emerged as the most viable route not only to grow highly crystalline 2D material films but also to directly grow covalently bonded, continuous 3D networks of those 2D materials.[1,16,17] For the latter, the CVD approach essentially relies on a 3D template that can be exposed to growth conditions at high enough temperatures to crystallise 2D materials on its surface. Most promising particularly for graphene, are thereby transition metal templates with catalytic properties that allow for the synthesis of highly crystalline graphene at relatively low temperatures.[17,18] While numerous methods to create suitable 3D metal templates have been demonstrated, ranging from commercial metal foams[1] and sintering of metal powders[4,5] to 3D printing[19] and two-photon lithography,[20] the bottleneck remains 3D template control and accessible size/resolution. Typical metal foams have pore diameters of the order of 100µm,[1] and over such large sizes mono-layer graphene is not self-supporting, i.e. when the metal template is etched away the structure easily collapses. The smallest pore sizes demonstrated to date are of the order of 1µm.[4,20] Most recently, nano-porous zeolites decorated with Lanthanum have been used as a template to create carbon frameworks, albeit not fully graphitised.[7] Further, computational modelling has recently highlighted the potential exceptional properties of periodic gyroid graphene structures.[13] A well-known challenge in particular for pure metal templates is their high self-diffusivity,[21] which means that metal templates of sub-100nm unit cell size are prone to sintering, i.e. are not stable, at the required elevated CVD temperatures.

Here, we demonstrate the direct CVD of freestanding graphene gyroids with controlled sub-60nm unit cell sizes. We use Ni gyroidal templates prepared through electrodeposition into a selectively voided triblock terpolymer.[22] The high temperature instabilities of sub-micron unit cell structures are avoided through the early introduction of the carbon precursor, which is found to stabilize the metallized gyroidal templates.[23] The as-grown graphene gyroids are self-supporting and can be transferred from the deposition substrate. We analyse their structure by electron microscopy and optical spectroscopy. We discuss the generality of our methodology for the synthesis of other types of freestanding 2D material assemblies on the sub-micron scale.

Results and Discussion

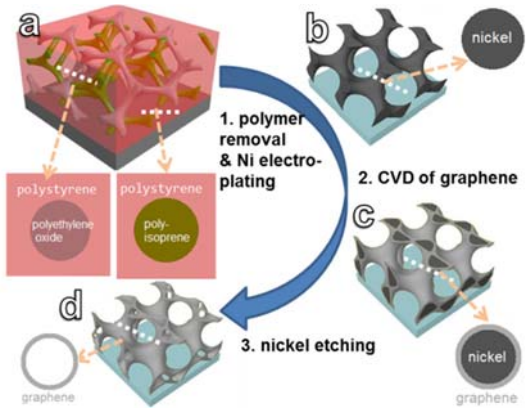

FIG. 1. (a) Schematic geometry and composition of alternating gyroid (gyroidal) phase of the ISO triblock copolymer: red – polystyrene matrix; blue – polyethylene oxide gyroid network; green – polyisoprene gyroid network. (b) Nickel gyroid prepared by electroplating into empty space left after polyisoprene removal. (c) Nickel gyroid covered in graphene after CVD with acetylene precursor. (d) Self-standing graphene gyroid after nickel removal with ferric chloride solution. Insets represent cross-sections of the respective structures along the indicated white line.

Figure 1 schematically highlights the synthesis process used to form freestanding graphene gyroids (see Methods in Supplementary Information for more details). The initial polymer templates are fabricated using a polyisoprene-b-polystyrene-poly(ethylene oxide) (ISO) triblock copolymer (Fig. 1a), which is composed of polyisoprene (PI), poly(ethylene oxide) (PEO), and polystyrene (PS).[22] Here we vary the molecular weights of the ISO to obtain polymer templates with different unit cell sizes. Polymer templates with a unit cell size of ~35nm are fabricated using ISO of ~33 kg/mol, while those with unit cell size of ~60nm are fabricated using ISO of ~80 kg/mol.[24] They are deposited on conductive fluorine-doped tin oxide (FTO)-coated glass and thermally annealed in a vacuum oven to form the desired microphase-separated morphology. PI is subsequently removed from the ISO polymer templates by UV exposure and an ethanol rinse. These polymer templates are then metallized by electroplating Ni into the voids left after PI removal, using the FTO-coated glass as a working electrode. The remaining polymers are subsequently removed by oxygen plasma etching. Polymer removal results in gyroidal Ni templates (denoted further as G35_Ni for 35nm unit cell size and G60_Ni for 60nm unit cell size) that structurally resemble the original polymer templates (Fig. 1b).[25] Graphene layers are then catalytically grown on the Ni surface by CVD (Fig. 1c). CVD is performed using pure acetylene (C_2H_2) as the precursor at $2.2x10^{-3}$mbar and heating to 550-650^{o}C, as discussed later for the optimised process. The resulting structures are denoted G60_Ni+G and G35_Ni+G. After CVD, the Ni is removed by $FeCl_3$ etching, resulting in freestanding graphene gyroids. Consequently these are denoted G60_G and G35_G. These graphene gyroids can then be easily transferred by etching the underlying FTO layer with HCl followed by gyroid lift-off and transfer onto a glass slide for rinsing in DI water and then eventually onto the desired substrate. As we show below, the as-fabricated graphene gyroids can be freestanding and are stable enough to support their own weight, hence the transfer can be achieved without additional polymer support, unlike in the standard graphene PMMA transfer (see Supplementary Information S.Ia).[26,27]

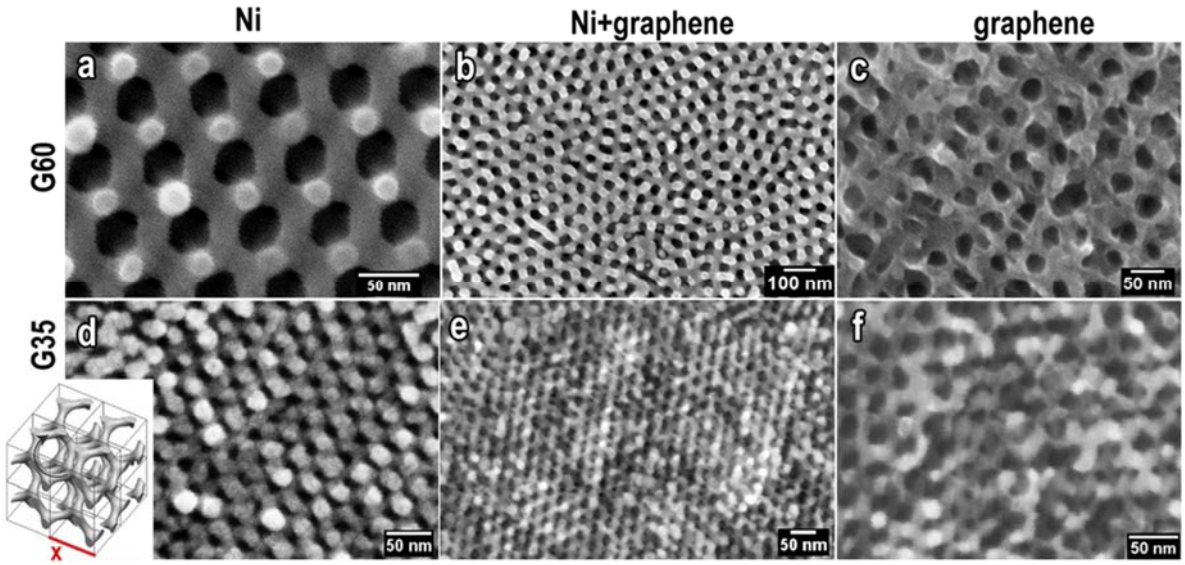

FIG. 2. Gyroids of two unit cell sizes: 60nm (G60) and 35nm (G35) analysed by SEM: (a) G60_Ni nickel template. (b) G60_Ni+G nickel template with graphene – after CVD. (c) Free standing graphene G60_G – after nickel etching. (d). G35_Ni nickel template. (e) G35_Ni+G nickel template with graphene – after CVD. (f) Free standing graphene G35_G – after nickel etching. The inset schematically highlights eight unit cells of the gyroid structure, whereby x is 60nm for G60 and 35nm for G35, respectively, in the used nomenclature.

Figure 2 shows SEM analysis of the gyroid structure at the various process stages. CVD allows freestanding graphene gyroids to be fabricated across large areas. As shown in Figure S.Ib (Supplementary Information), graphene gyroids can be readily fabricated over cm^2 areas. Optically, freestanding graphene gyroids are similar in appearance to the nickel templates, although they appear less opaque (Fig. S.IIa-d). SEM images show that both G60_G and G35_G have successfully inherited the shape and scale of their respective nickel templates – G60_Ni and G35_Ni, with the unit cells of ~60nm and ~35nm (Fig. 2a-c, Fig. 2d-f, respectively). EDX spectra (Fig. S.IIe) show no Ni peak, consistent with the removal of Ni. The O, Si and Sn peaks in the graphene gyroid EDX spectrum originate from the underlying FTO glass, and are more prominent than for the nickel gyroids, due to the higher electron and x-ray transparency of the graphene gyroids.[28,29] Nickel X-ray excitation energies are Kα = 7.480 keV and Lα = 0.849 keV. With 12 kV acceleration energy the Lα peak is prominent and Kα weak. These peaks are not observed at all in the graphene gyroids' EDX. The graphene gyroids display good electrical properties – G60_G transferred on non-conductive glass exhibits a sheet resistance of 240 Ω/□, with the gyroid film having the thickness of ~500nm (see Supplementary Information for details).

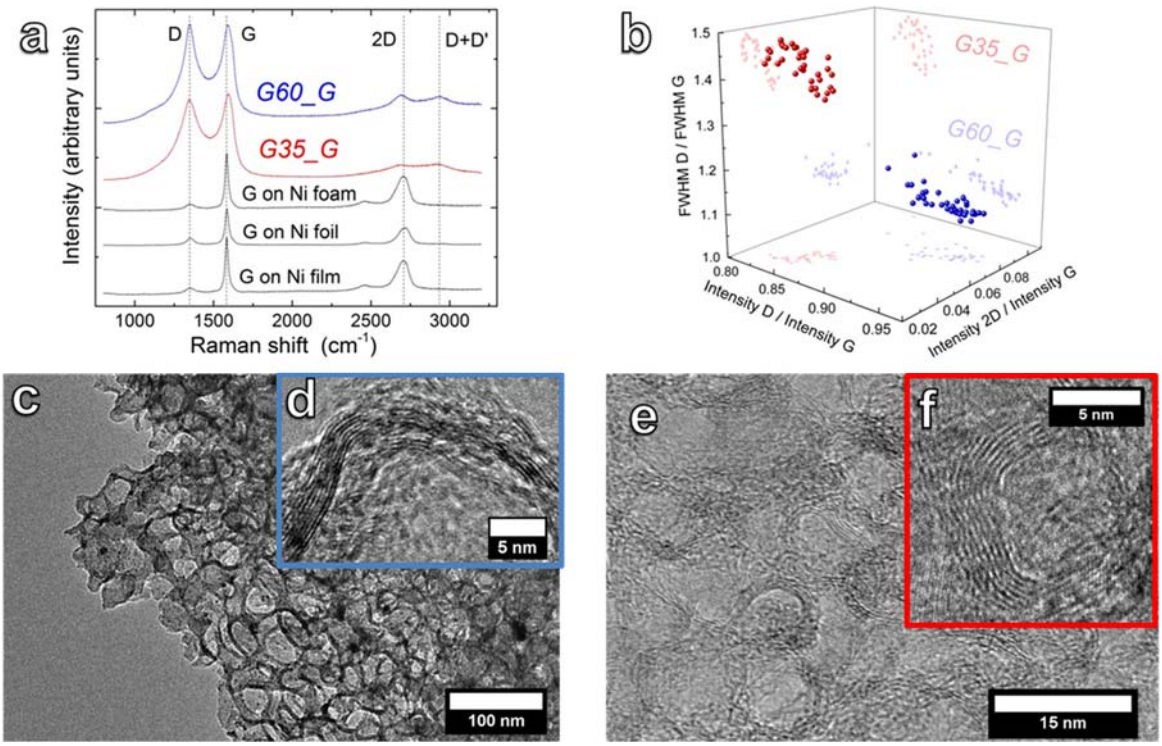

FIG. 3. (a) Raman spectra of: graphene on 500nm Ni film (bottom black line), graphene on 25µm Ni foil (middle black line), graphene on Ni foam (top black line), G35_G (red line) and G60_G (blue line). (b) 3D plot of ratio of intensities of D/G versus intensities 2D/G peaks versus ratio of full width at half maximum of D/G peaks in Raman mapping of G35_G (red data points) and G60_G (blue data points). Shaded spots are projections of data onto given plane. Each mapping contains 36 measurements spanning 25x25µm area. HRTEM images of (c) G60_G. (d) Close up on one of the G60_G channels, the channel diameter is ~15nm (e) G35_G. (f) Close up of one of the G35_G channels, the channel diameter is ~5nm.

The Raman spectra in Figure 3a, compare G60_G with graphene deposited on Ni foam (~100µm pore size)[1], Ni foil (25 µm) and Ni film (500 nm), under similar conditions, the major difference being the heat conductivity and thickness of the substrates. G60_G is also compared with G35_G deposited at lower temperature. The Raman spectra of the graphene deposited on 3D gyroidal structures differ significantly from those of the graphene deposited on flat substrates, despite the growth conditions remaining unchanged. The Raman spectra of foam, foil and film are characteristic of flat, few-layer graphene.[30] In contrast, the spectra of G60_G and G35_G display prominent and wide D and G peaks with intensities ratio I_D/I_G ~1. The prominence of the D peaks in both G60_G and G35_G is attributable to the presence of many small and disordered graphene domains.[31,32] The G band for the gyroids appears at higher wavenumber than for the flat substrates which is consistent with the presence of strained nanosized graphene layers.[33] Figure 3b presents a 3D plot of I_D/I_G vs. I_{2D}/I_G vs. $FWHM_D$ / $FWHM_G$ (ratio of width of the peaks, presented as ratio of full widths at half maximums). The plot has two separated clusters of data points indicating a significant difference between G35_G and G60_G. We suggest that this results from the different radius of curvatures of the supports on which the graphene conformally grows. The lower I_{2D}/I_G for G35_G can be attributed to larger strain present in double C=C bonds chains due to the higher curvature.[34] Broadening of the D peak, shown by both higher $FWHM_D$ / $FWHM_G$ and lower I_D/I_G for G35_G, could indicate higher disorder caused by smaller grain size and higher number of non-six member rings required to conform to the

curvature.[35] This is also consistent with the fact (discussed below) that in G35_G grown at lower temperatures, recrystallization, self-healing and merging of domains could not happen to the same extent as in G60_G. Finally, it is prudent to mention that the Ni in the gyroids comes from a electroplating solution, which might contain trace amounts of levelling agents and other impurities. These, even though present in very small amounts, may affect the nucleation density. However, a more detailed analysis is beyond the scope of this paper.

Figure 3c-f shows TEM images of G60_G (Fig. 3c,d) and G35_G (Fig. 3e,f). It is evident that the structures are graphitic with few-layered graphene forming the walls of the channels. The observed crystal quality is consistent with the Raman results discussed above. The radii of the G60_G pores are ~15nm, with about 10 layers forming the walls (Fig. 3d), similarly the G35_G has pore radii of ~5nm and also about 10 layers forming the walls (Fig. 3f). Both results are consistent with the geometry of gyroids (Fig. 2 inset). The lattice spacing observed in the TEM images is about 0.335nm which corresponds well to the interlayer spacing of graphite.[36]

Figure 4 demonstrates the main challenge regarding CVD using a nanoscale metal template - the instability of the metal catalyst at high temperatures. Unlike Ni foam templates with unit cell sizes of the order of hundreds of microns,[1] the sub-micron unit cells of Ni gyroid templates transform into bulky clusters at temperatures >500°C. The formation of clusters is driven by the thermodynamic tendency to minimise the surface area and is made possible by the increase in Ni self-diffusion with temperature.[37] Using a typical one-step CVD process,[18] where the hydrocarbon precursor is introduced only once the growth temperature has been reached, both G35_Ni and G60_Ni do not preserve their original morphologies and already transform during the heating ramp into lower energy configurations, i.e. clusters (Fig. 4a). To overcome this limitation, we introduce the carbon precursor right from the beginning of the heating ramp (predosing), which helps to stabilize the nickel templates and prevent the formation of Ni clusters at growth temperature (Fig. 4b). We believe that the following mechanisms play a role in stabilising the template: During the initial heating of the template, precursor dissociation begins well below the maximum process temperature, with the supplied C being readily absorbed by the Ni template, given the reasonably large solubility of C in Ni.[38] When the Ni surface becomes filled with C beyond its solubility limit, the additional hydrocarbon dissociation feeds graphene nucleation at the Ni surface.[39] The relatively small bulk of the gyroids compared to thicker catalyst foams, foils, and films means this point is reached at a lower temperature. Consistent with Raman results discussed above, a higher nucleation density is thus expected as a result of the lower C diffusivity at this low nucleation temperature,[18] as well as the higher template curvature and thus abundance of low-coordination sites which serve as preferential nucleation sites. This promotes the formation of small graphene islands of low graphitic quality which continue to grow isothermally as the precursor exposure continues to form a continuous graphitic network over the template.[40] These graphitic deposits are expected to exhibit a strong interaction with the Ni, as a result of hybridisation between the graphene π and Ni 3d orbitals, and thus help to stabilise the template.[41] Additionally, nickel surface carbides are known to readily form on Ni at temperatures <500 °C,[42] which may also assist in stabilising the template. As the process temperature continues to increase, amorphous and highly defective regions of the C coating are graphitised, which may involve defect healing as well as a re-dissolution process as the C solubility in Ni increases with temperature. This ultimately yields the crystalline graphitic layers presented in the TEM images of Figure 3.

Our approach can be extended both to other metal templates and to materials beyond graphene. For a given metal template our approach will depend on its catalytic efficiency to induce graphitisation versus its self-diffusivity at the given temperature. Hence the temperature instabilities of sub-micron unit cell structures can be similarly addressed for metals that in those respects show similar behaviour to Ni,[37] such as Co,[43] or for metals, that require higher growth temperatures but have lower self-diffusivity, such as Pt.[44–46] For metals, such as Cu, that both require higher growth temperatures for graphene growth and have high self-diffusivity (3 orders of magnitude higher for Cu than Ni at 900°C),[47,48] our approach will be more challenging. Nonetheless there are further avenues to increase template stability for instance via plasma pre-coating in these cases. The challenge for 3D structural control is common to many different materials beyond graphene, including for instance ceramic foams. Ceramic foam structures, particularly based on thermally and chemically stable boron nitride, have a wide application potential, ranging from mechanical metamaterials[49] to filtration and catalysis.[50] The templated CVD approach can be expanded to fabricate free-standing hexagonal boron nitride (h-BN) gyroid structures. The template stabilisation for h-BN CVD is more complex to rationalise as the supply, solubility and chemical behaviour of both B and N with respect to the catalyst template have to be considered. This connects to our previous detailed h-BN growth studies,[51,52] however a detailed discussion of this goes beyond the scope of this paper. Equally without discussing the growth mechanisms involved, our approach can be extended to transition metal dichalcogenides, for instance by using Au gyroids for WS_2 CVD.[53]

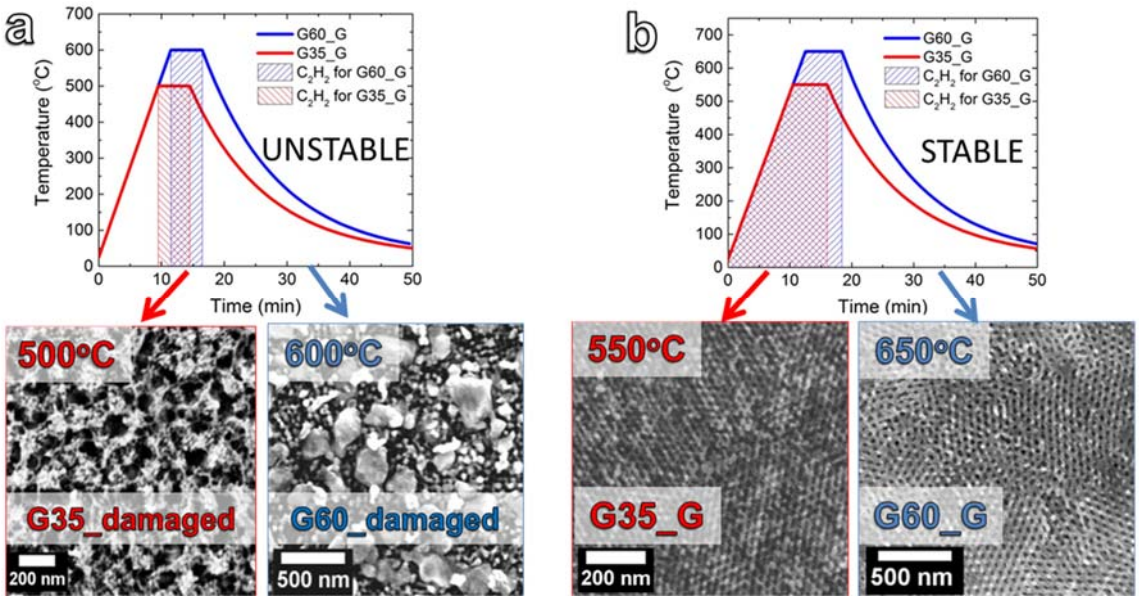

FIG. 4. Process diagrams presenting unstable (a) and stable (b) procedures for graphene gyroids preparation. Structures in (b) are stabilised by acetylene (gas precursor) preloading at RT; SEM images in (a) show damage to G35 and G60 at as low as 500°C and 600°C respectively; SEM images in (b) show preserved G35_G and G60_G after processing in 550°C and 650°C respectively; The process diagram in (b) also presents the optimal conditions for graphene gyroids preparation via CVD.

Conclusions

We demonstrated the successful fabrication of sub-60nm pore-size graphene gyroids, produced via an optimised CVD process using sub-micron scale Ni templates which were prepared through the use of electrodeposition within a selectively voided triblock terpolymer. The resulting freestanding graphene gyroids of two unit cell sizes, 35 and 60nm, replicate the original template structure and show reasonable graphitic crystal quality. The early introduction of the carbon precursor allowed us to effectively address the high temperature instabilities of sub-micron unit cell structures. We discussed how this approach can be extended both to other metal templates and to materials beyond graphene. We highlighted how for a given template the approach relies on its catalytic efficiency to induce 2D material growth versus its self-diffusivity/thermal stability. The demonstrated control of such novel foam-like materials on the sub-micron scale opens novel or enhanced functionality for a wide range of emerging applications where light-weight, high surface area, mechanical stability is desirable.

Acknowledgements

We acknowledge funding from EPSRC (Grant No. EP/K016636/1, GRAPHTED) and ERC (Grant No. 279342, InsituNANO, and 259619, PHOTO EM), as well as Cambridge University NanoDTC (Grant No. EPSRC EP/G037221/1). R.S.W. acknowledges a Research Fellowship from St. John's College, Cambridge and a EU Marie Skłodowska-Curie Individual Fellowship under grant ARTIST (no. 656870).

References

[1] Z. Chen, W. Ren, L. Gao, B. Liu, S. Pei, and H.-M. Cheng, Nat. Mater. **10**, 424 (2011).
[2] Y. Ito, Y. Tanabe, H. Qiu, K. Sugawara, S. Heguri, N.H. Tu, K.K. Huynh, T. Fujita, T. Takahashi, K. Tanigaki, and M. Chen, Angewandte **53**, 4822 (2014).
[3] C. Hou, T. Huang, H. Wang, H. Yu, Q. Zhang, and Y. Li, Sci. Rep. **3**, 3138 (2013).
[4] S. Drieschner, M. Weber, J. Wohlketzetter, J. Vieten, E. Makrygiannis, B.M. Blaschke, V. Morandi, L. Colombo, F. Bonaccorso, and J.A. Garrido, 2D Mater. **3**, 45013 (2016).
[5] J. Sha, C. Gao, S.K. Lee, Y. Li, N. Zhao, and J.M. Tour, ACS Nano **10**, 1411 (2016).
[6] K. Xi, P.R. Kidambi, R. Chen, C. Gao, X. Peng, C. Ducati, S. Hofmann, and R.V. Kumar, Nanoscale **6**, 5746 (2014).
[7] K. Kim, T. Lee, Y. Kwon, Y. Seo, J. Song, J.K. Park, H. Lee, J.Y. Park, H. Ihee, S.J. Cho, and R. Ryoo, Nature **535**, 131 (2016).
[8] M.T. Pettes, H. Ji, R.S. Ruoff, and L. Shi, Nano Lett. **12**, 2959 (2012).
[9] E. Singh, Z. Chen, F. Houshmand, W. Ren, Y. Peles, H.-M. Cheng, and N. Koratkar, Small **9**, 2 (2013).
[10] H. Bi, X. Xie, K. Yin, Y. Zhou, S. Wan, L. He, F. Xu, F. Banhart, L. Sun, and R.S. Ruoff, Adv. Funct. Mater. **22**, 4421 (2012).
[11] J. Liu, X. Wang, T. Wang, D. Li, F. Xi, J. Wang, and E. Wang, ACS Appl. Mater. Interfaces **6**, 19997 (2014).
[12] A.E. Jakus, E.B. Secor, A.L. Rutz, S.W. Jordan, and M.C. Hersam, ACS Nano **9**, 4636 (2015).
[13] Z. Qin, G.S. Jung, M.J. Kang, and M.J. Buehler, Sci. Adv. 1 (2017).
[14] L. Qiu, J.Z. Liu, S.L.Y. Chang, Y. Wu, and D. Li, Nat. Commun. **3**, 1241 (2012).
[15] P.C. Sherrell and C. Mattevi, Mater. Today **19**, 428 (2016).
[16] M. Mecklenburg, A. Schuchardt, Y.K. Mishra, S. Kaps, R. Adelung, A. Lotnyk, L. Kienle, and K. Schulte, Adv. Mater. **24**, 3486 (2012).
[17] S. Hofmann, P. Braeuninger-Weimer, and R.S. Weatherup, J. Phys. Chem. Lett. **6**, 2714 (2015).
[18] R.S. Weatherup, B.C. Bayer, R. Blume, C. Ducati, C. Baehtz, R. Schl, and S. Hofmann, Nano Lett. **11**, 4154 (2011).
[19] Z. Yang, C. Yan, J. Liu, S. Chabi, Y. Xia, and Y. Zhu, RSC Adv. **5**, 29397 (2015).
[20] J. Bauer, A. Schroer, R. Schwaiger, and O. Kraft, Nat. Mater. **15**, 438 (2016).
[21] Landolt-Börnstein, *Diffusion in Solid Metals and Alloys* (1990).
[22] S. Vignolini, N.A. Yufa, P.S. Cunha, S. Guldin, I. Rushkin, M. Stefik, K. Hur, U. Wiesner, J.J. Baumberg, and U. Steiner, Adv. Mater. **24**, 23 (2012).
[23] B.C. Bayer, D.A. Bosworth, F.B. Michaelis, R. Blume, G. Habler, R. Abart, R.S. Weatherup, P.R. Kidambi, J.J. Baumberg, A. Knop-Gericke, R. Schloegl, C. Baehtz, Z.H. Barber, J.C. Meyer, and S. Hofmann, J. Phys. Chem. C **120**, 22571 (2016).
[24] S. Salvatore, A. Demetriadou, S. Vignolini, S.S. Oh, S. Wuestner, N.A. Yufa, M. Stefik, U. Wiesner, J.J. Baumberg, O. Hess, and U. Steiner, Adv. Mater. **25**, 2713 (2013).
[25] J.A. Dolan, M. Saba, R. Dehmel, I. Gunkel, Y. Gu, U. Wiesner, O. Hess, T.D. Wilkinson, J.J. Baumberg, U. Steiner, and B.D. Wilts, ACS Photonics **3**, 1888 (2016).
[26] A. Reina, H. Son, L. Jiao, B. Fan, M.S. Dresselhaus, Z. Liu, and J. Kong, Phys. Chem. C **112**, 17741 (2008).
[27] M. Kratzer, B.C. Bayer, P.R. Kidambi, A. Matković, R. Gajić, A. Cabrero-Vilatela, R.S. Weatherup, S. Hofmann, and C. Teichert, Appl. Phys. Lett. **106**, (2015).
[28] R.S. Weatherup, B. Eren, Y. Hao, H. Bluhm, and M.B. Salmeron, J. Phys. Chem. Lett. **7**, 1622 (2016).
[29]http://henke.lbl.gov/cgi (n.d.).
[30] A.C. Ferrari, J.C. Meyer, V. Scardaci, C. Casiraghi, M. Lazzeri, S. Piscanec, K.S. Novoselov, S. Roth, and A.K. Geim, Phys Rev Lett. **97**, 187401 (2006).
[31] J. Biener, S. Dasgupta, L. Shao, D. Wang, M.A. Worsley, A. Wittstock, J.R.I. Lee, M.M. Biener, C.A. Orme, S.O. Kucheyev, B.C. Wood, T.M. Willey, A. V Hamza, J. Weissmüller, H. Hahn, and T.F. Baumann, Adv. Mater. **24**, 5083 (2012).
[32] M.A. Pimenta, G. Dresselhaus, M.S. Dresselhaus, and L.G. Canc, Phys. Chem. Chem. Phys. **9**, 1276 (2007).
[33] G. Ning, Z. Fan, G. Wang, and J. Gao, Chem. Comm **47**, 5976 (2011).
[34] A.C. Ferrari and J. Robertson, Phys. Rev. B **64**, 75414 (2001).
[35] A.C. Ferrari and J. Robertson, Phys. Rev. B **61**, 14095 (2000).
[36] G.E. Bacon, Acta. Cryst. **4**, 558 (1951).
[37] W.S. K. Maier, H. Mehrer, E. Lessmann, Phys. Stat. Sol. **78**, 689 (1976).
[38] J.J. Lander, H.E. Kern, and A.L. Beach, J. Appl. Phys. **23**, 1305 (1952).
[39] R.S. Weatherup, C. Baehtz, B. Dlubak, B.C. Bayer, P.R. Kidambi, R. Blume, R. Schloegl, and S. Hofmann, Nano Lett. **13**, 4624 (2013).

[40] R.S. Weatherup, B.C. Bayer, R. Blume, C. Baehtz, P.R. Kidambi, M. Fouquet, C.T. Wirth, R. Schlögl, and S. Hofmann, Chemphyschem **13**, 2544 (2012).
[41] R.S. Weatherup, L.D. Arsie, A. Cabrero-vilatela, S. Caneva, R. Blume, J. Robertson, R. Schloegl, and S. Hofmann, JACS **137**, 14358 (2015).
[42] L.L. Patera, C. Africh, R.S. Weatherup, R. Blume, S. Bhardwaj, C. Castellarin-cudia, A. Knop-gericke, R. Schloegl, G. Comelli, and S. Hofmann, ACS Nano **7**, 7901 (2013).
[43] A. Cabrero-Vilatela, R.S. Weatherup, P. Braeuninger-Weimer, S. Caneva, and S. Hofmann, Nanoscale **8**, 2149 (2016).
[44] R.S. Weatherup, A.J. Shahani, Z. Wang, K. Mingard, A.J. Pollard, M. Willinger, R. Schloegl, P.W. Voorhees, and S. Hofmann, Nano Lett. **16**, 6196 (2016).
[45] F. Cattaneo, E. Germagnoli, and F. Grasso, Philos. Mag. **7**, 1373 (1962).
[46] A.J. Melmed, J. Appl. Phys. **38**, 1885 (1967).
[47] P.R. Kidambi, C. Ducati, B. Dlubak, D. Gardiner, R.S. Weatherup, M.-B. Martin, P. Seneor, H. Coles, and S. Hofmann, J. Phys. Chem. C **116**, 22492 (2012).
[48] C.T.T. A. Kuper, H. Letaw, L. Slifkin, E. Sonder, Phys. Rev. **96**, 1224 (1954).
[49] J. Yin, X. Li, J. Zhou, and W. Guo, Nano Lett. **13**, 3232 (2013).
[50] J.G. Alauzun, S. Ungureanu, N. Brun, S. Bernard, P. Miele, R. Backov, and C. Sanchez, J. Mater. Chem **21**, 14025 (2011).
[51] S. Caneva, R.S. Weatherup, B.C. Bayer, B. Brennan, S.J. Spencer, K. Mingard, A. Cabrero-vilatela, C. Baehtz, A.J. Pollard, and S. Hofmann, Nano Lett. **15**, 1867 (2015).
[52] P.R. Kidambi, R. Blume, J. Kling, J.B. Wagner, C. Baehtz, R.S. Weatherup, R. Schloegl, B.C. Bayer, and S. Hofmann, Chem. Mater. **26**, 6380 (2014).
[53] Y. Gao, Z. Liu, D. Sun, L. Huang, L. Ma, L. Yin, and T. Ma, Nat. Commun. **6**, 8569 (2015).